

# Rich quantum phases in the anisotropic sub-Ohmic spin-boson model

Yan-Zhi Wang<sup>1</sup>, Shu He<sup>2</sup>, Liwei Duan<sup>1</sup>, and Qing-Hu Chen<sup>1,3,\*</sup>

<sup>1</sup> *Department of Physics and Zhejiang Province Key Laboratory of Quantum Technology and Device, Zhejiang University, Hangzhou 310027, China*

<sup>2</sup> *Department of Physics and Electronic Engineering, Sichuan Normal University, Chengdu 610066, China*

<sup>3</sup> *Collaborative Innovation Center of Advanced Microstructures, Nanjing University, Nanjing 210093, China*

(Dated: January 8, 2020)

We study the anisotropic spin-boson model (SBM) by a numerically exact method based on variational matrix product states. Rich phase diagram is found in the anisotropy-coupling strength plane by calculating several observables. There are three distinct quantum phases: delocalized phase with even parity (phase I), delocalized phase with odd parity (phase II), and localized phase with broken  $Z_2$  symmetry (phase III), which intersect at a quantum tricritical point. The competition between those phases will give overall picture of the phase diagram. For small bath exponent in the regime of  $s < 1/2$ , the quantum phase transition (QPT) from phase I to III with mean-field critical behaviors is present, similar to the isotropic SBM. The novel phase diagram full with three different phases can be only found at large bath exponent for  $s > 1/2$ : For highly anisotropic case, the system will undergo the QPTs from phase I to II via 1st-order, and then to the phase III via 2nd-order with the coupling strength. For low anisotropic case, the system only experiences the continuous QPT from phase I to phase III with the non-mean-field critical exponents. Very interestingly, at the moderate anisotropy, the system would display the continuous QPTs for several times but with the same critical exponents. This unusual reentrance to the same localized phase is first discovered in the light-matter interacting systems. Thus, the anisotropic SBM would be potential interesting platform to study the rich quantum criticality.

PACS numbers: 03.65.Yz, 03.65.Ud, 71.27.+a, 71.38.k

## I. INTRODUCTION

Quantum phase transition (QPT) has been studied for many years and continues to be the hot topics in many correlated matters and the light-matter interacting systems [1], such as the fermionic [2], spin [1], bosonic [3], as well as the fermion (spin)-boson coupling systems [4, 5]. Because fermions have both the spin and charge degree of freedom, so the rich and novel quantum phases can emerge in the fermions models and bosonic model where bosons are formed by composite fermions or cold atoms in the strongly correlated system.

In the light-matter interacting systems, many prototype models such as the quantum Rabi model [6], the Dicke model [7], and the spin-boson model (SBM)[5] only experience a single QPT from the normal to superradiant phase for the single mode bosonic cavity or delocalized to localized phase for the bosonic bath. The QPT of most models are trivially of the mean-field nature. Only the sub-Ohmic SBM can also display the non-mean-field critical behavior with large power of the spectral function of the bosonic bath [8]. The nonclassical critical behavior is at the heart of so-called local quantum criticality [9].

To obtain the rich phase diagram, the generalized Dicke models, such as the anisotropic Dicke model [10, 11], the anisotropic Dicke model with the Stark coupling terms [12], and the staggered Dicke model [13] have been recently studied by several groups. A quantum tricritical point [14] is seldomly supported in the solid-state materials, and is almost impossible to appear in the prototype models in the light-matter interacting systems.

Interestingly, it has been found to exist in anisotropic Dicke model [11] and the isotropic Dicke model with staggered fields [13]. In the former model, the quantum tricritical point lies at the symmetric line of the super-radiant “electric” and “magnetic” phases which can be switched mutually by interchanging the coupling parameters. While in the latter model, the 1st-order critical line meets the 2nd-order one at the quantum tricritical point. Yet it has not been found that three critical lines intersect at the quantum tricritical point and separate three phase in an asymmetric way as in the  $He^3 - He^4$  mixture [14] in the light-matter interacting systems until now, to the best of our knowledge.

The phase diagrams in these generalized Dicke models become richer than their prototype models, but still only includes one 1st-order and one 2nd-order critical lines, possibly due to the fact that only a single phase transition with mean-field type is present in the prototype models. This situation might be changed in a generalized model if its prototype one can exhibit the non-mean-field critical behavior, like the sub-Ohmic SBM.

As is well known that the SBM is a paradigmatic model in many fields, ranging from quantum optics [15], to condensed matter physics [5], to open quantum systems [16, 17]. With the advance of modern technology, various qubit and oscillator coupling systems can be engineered in many solid-state devices, such as superconducting circuits [18, 19], cold atoms [20], and trapped ions [21]. Recently, the SBM has been realized by the ultrastrong coupling of a superconducting flux qubit to an open one-dimensional (1D) transmission line [22]. The counterro-

tating terms can be suppressed in some proposed schemes [10, 23, 24]. In some systems, the anisotropy appears quite naturally, because they are controlled by different input parameters [25].

In the sub-Ohmic SBM, the 2nd-order QPT from the delocalized phase, where spin has the equal probability in the two states, to localized phase, in which spin prefers to stay in one of the two states, has been studied extensively [8, 26–34]. Unlike the Dicke model and the quantum Rabi model, the SBM has various universality classes, depending on the power of the spectral function of the bosonic bathes, its generalized model including anisotropy might support richer quantum phases with the help of the additional parameter dimension.

In this paper, we will extend the variational matrix product state (VMPS) approach [31] to study the anisotropic spin-boson model (ASBM) with the sub-Ohmic bath. The multi-coherent state (MCS) variational approach is also employed to provide independent checks of the emerged new phase. The paper is organized as follows. In Sec. II, we introduce the ASBM. Some methodologies including the VMPS, the MCS variational approaches are reviewed briefly. The rich phase diagrams revealed by the VMPS method are presented in Sec. III. A quantum tricritical point is observed and the quantum criticality based on VMPS studies for the parity, the order parameter, and the entanglement entropy is also analyzed. Finally, conclusions are drawn in Sec. IV.

## II. GENERALIZED MODEL HAMILTONIAN AND METHODOLOGIES

The ASBM Hamiltonian can be written as ( $\hbar = 1$ )

$$\hat{H} = \frac{\Delta}{2}\sigma_z + \frac{\epsilon}{2}\sigma_x + \sum_k \omega_k a_k^\dagger a_k + \frac{1}{2} \sum_k g_k \left( a_k^\dagger + a_k \right) \sigma_x + \frac{\lambda}{2} \sum_k g_k \left( a_k - a_k^\dagger \right) i\sigma_y, \quad (1)$$

where  $\sigma_i$  ( $i = x, y, z$ ) are the Pauli matrices,  $\Delta$  is the qubit frequency,  $\epsilon$  is the energy bias applied in a two-level system, and  $\lambda$  reflects the degree of anisotropy in this model with  $0 < \lambda < 1$ .  $a_k$  ( $a_k^\dagger$ ) is the bosonic annihilation (creation) operator which can annihilate (create) a boson with frequency  $\omega_k$ , and  $g_k$  denotes the coupling strength between the qubit and the bosonic bath, which is usually characterized by the power-law spectral density  $J(\omega)$ ,

$$J(\omega) = \pi \sum_k g_k^2 \delta(\omega - \omega_k) = 2\pi\alpha\omega_c^{1-s}\omega^s \Theta(\omega_c - \omega), \quad (2)$$

where  $\alpha$  is a dimensionless coupling constant,  $\omega_c$  is the cutoff frequency, and  $\Theta(\omega_c - \omega)$  is the Heaviside step function. The power of the spectral function  $s$  classifies the reservoir into super-Ohmic ( $s > 1$ ), Ohmic ( $s = 1$ ), and sub-Ohmic ( $s < 1$ ) types. On the one hand, the isotropic SBM can be described by Hamiltonian (1) with

$\lambda = 0$ . On the other hand, if the counterrotating terms involving higher excited states,  $a_k^\dagger\sigma_+$  and  $a_k\sigma_-$  are neglected ( $\lambda = 1$ ), the ASBM is reduced to the SBM in the rotating-wave approximation (RWA), which has been studied by the present authors recently [35].

The ASBM possesses a  $Z_2$  symmetry, similar to the isotropic SBM model. The parity operator is defined as

$$\hat{\Pi} = \exp\left(i\pi\hat{N}\right), \quad (3)$$

where  $\hat{N} = \sum_k a_k^\dagger a_k + \sigma_+\sigma_-$  with  $\sigma_\pm = (\sigma_x \pm i\sigma_y)/2$  is the operator of the total excitation number. The parity operator  $\hat{\Pi}$  has two eigenvalues  $\pm 1$ , corresponding to even and odd parity in the symmetry conserved phases. The average value of the parity may become also zero due to the quantum fluctuations in the symmetry broken phase. So the parity can be employed to distinguish different phases in the ASBM.

*VMPS approach.* To apply VMPS in the ASBM, firstly the logarithmic discretization of the spectral density of the continuum bath [8] with discretization parameter  $\Lambda > 1$  is performed, followed by using orthogonal polynomials as described in Ref. [36], the ASBM can be mapped into the representation of a one-dimensional semi-infinite chain with nearest-neighbor interaction [37]. Thus, Hamiltonian (1) can be written as:

$$H_{\text{chain}} = \frac{\Delta}{2}\sigma_z + \frac{\epsilon}{2}\sigma_x + \frac{c_0}{2}(b_0 + b_0^\dagger)\sigma_x + \lambda\frac{c_0}{2}(b_0 - b_0^\dagger)i\sigma_y + \sum_{n=0}^{L-2} [\epsilon_n b_n^\dagger b_n + t_n (b_n^\dagger b_{n+1} + b_{n+1}^\dagger b_n)], \quad (4)$$

where  $b_n^\dagger$  ( $b_n$ ) is the creation (annihilation) operator for a new set of boson modes in a transformed representation with  $\epsilon_n$  describing frequency on chain site  $n$ ,  $t_n$  describing the nearest-neighbor hopping parameter, and  $c_0$  describing the effective coupling strength between the spin and the new effective bath. For details, one may refer to Ref. [36].

Then as introduced in [38, 39], we employ the standard matrix product representation with optimized boson bias  $|\tilde{n}_k\rangle$  through an additional isometric map with truncation number  $d_{\text{opt}} \ll d_n$  like in Refs. [31, 37] to study the quantum criticality of ASBM. Each site in the 1D chain can be described by the matrix  $M$ , which is optimized through sweeping the 1D chain iteratively to obtain the ground state, and  $D_n$  is the bond dimension for matrix  $M$  with the open boundary condition, bounding the maximal entanglement in each subspace.

For the data presented below, we typically choose the same model parameters in Ref. [31, 35], as  $\Delta = 0.1$ ,  $\omega_c = 1$ ,  $\epsilon = 0$ , the logarithmic discretization parameter  $\Lambda = 2$ , the length of the semi-infinite chain  $L = 50$ , and optimized truncation numbers  $d_{\text{opt}} = 12$ . In addition, we adjust the bond dimension as  $D_{\text{max}} = 20, 40$  for  $s = 0.3, 0.7$ , respectively, which is sufficient to obtain the converged results.

*MCS ansatz.*- We also apply the MCS ansatz [40, 41] to the ASBM. To facilitate the variational study and visualize the symmetry breaking explicitly, we rotate the Hamiltonian (1) around the  $y$  axis by an angle  $\pi/2$  with  $\epsilon = 0$ , which gives

$$H^T = -\frac{\Delta}{2}\sigma_x + \sum_k \omega_k a_k^\dagger a_k + \frac{1}{2} \sum_k g_k (a_k^\dagger + a_k) \sigma_z + \frac{\lambda}{2} \sum_k g_k (a_k - a_k^\dagger) i\sigma_y. \quad (5)$$

The trial state  $|\psi^T\rangle$  is written in the basis of the spin-up state  $|\uparrow\rangle$  and spin-down state  $|\downarrow\rangle$

$$|\psi^T\rangle = \begin{pmatrix} \sum_{n=1}^{N_c} A_n \exp \left[ \sum_{k=1}^L f_{n,k} (a_k^\dagger - a_k) \right] |0\rangle \\ \sum_{n=1}^{N_c} B_n \exp \left[ \sum_{k=1}^L h_{n,k} (a_k^\dagger - a_k) \right] |0\rangle \end{pmatrix}, \quad (6)$$

where  $A_n$  ( $B_n$ ) is related to the occupation probability of the spin-up (spin-down) state in the  $n$ th coherent state;  $N_c$  and  $L$  are numbers of coherent states and total bosonic modes, respectively; and  $f_{n,k}$  ( $h_{n,k}$ ) represents bosonic displacement of the  $n$ th coherent state and  $k$ th bosonic mode. The symmetric MCS ansatz ( $A_n = \pm B_n$  with  $\pm$  denotes the even and odd parity and  $f_{n,k} = -g_{n,k}$ ) can only be applied to the delocalized phase, so one can easily detect the symmetry breaking.

The energy expectation value can be calculated as follows

$$E = \frac{\langle \psi^T | H^T | \psi^T \rangle}{\langle \psi^T | \psi^T \rangle}. \quad (7)$$

Minimizing the energy expectation value with respect to variational parameters gives the self-consistent equations, which in turn give the ground-state energy and wave function. It has been demonstrated that this wave function with at least a hundred of coherent states can describe the localized phase of the SBM [42].

The information of the ground-state can be also described by the Von Neumann entropy  $S_E$  of the ASBM, which characterizes the entanglement between spin and the bosonic bath

$$S_E = -Tr(\rho_{spin} \log \rho_{spin}), \quad (8)$$

where  $\rho_{spin}$  is the reduced density matrix for the spin.

For both VMPS and MCS approaches described above, discretization of the energy spectrum of the continuum bath should be performed at the very beginning in the practical calculations. The same logarithmic discretization is taken for both approaches if comparison is made below.

### III. RESULTS AND DISCUSSIONS

#### A. The phase diagram

It is generally accepted that isotropic SBM exhibits the mean-field critical behavior for  $s < 1/2$ , and the non-

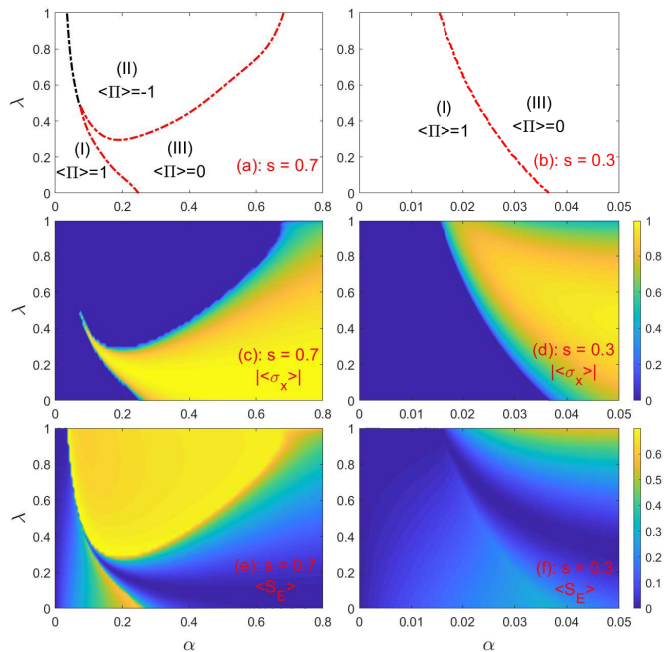


FIG. 1: (Color online) (upper panel) Phase diagram in the  $\alpha - \lambda$  plane for the ASBM drawn from the Parity (II): delocalized phases with even (I) and odd parity (II) with conserved  $Z_2$  symmetry, and the localized phase (III) with broken  $Z_2$  symmetry. (middle panel) Order parameter  $|\langle \sigma_x \rangle|$ . (lower panel) Entanglement entropy  $\langle S_E \rangle$ . The power of the spectral function is (left)  $s = 0.7$  and (right)  $0.3$ .  $\Delta = 0.1$ ,  $\omega_c = 1$ . The parameter used in the VMPS approach are  $\Lambda = 2$ ,  $L = 50$ ,  $d_{opt} = 12$ , and  $D = 20, 40$  for  $s = 0.3, 0.7$ , respectively.

classical one for  $s > 1/2$ , so we focus on two typical powers of the spectral function  $s = 0.7$  and  $0.3$  in this work. The main results for the ASBM based on the VMPS approaches are presented in Fig. 1 for  $s = 0.7$  (left) and  $0.3$  (right). Because the different phases in the ASBM can be precisely characterized by the parity. We therefore can compose the ground-state phase diagrams in the anisotropy  $\lambda$  and the coupling strength  $\alpha$  plane in the upper panel. We call phase I and II as the two delocalized ones with  $\langle \Pi \rangle = \pm 1$ , respectively, and phase III as the localized phase with  $\langle \Pi \rangle = 0$ . The boundary between the phase I and II is marked with the black dashed line, and the boundary of the phase III and the localized phases is indicated with the red dashed line. Clearly for  $s = 0.7$ , we really observe three phases full with the phase diagram and a quantum tricritical point is the intersecting point of the three critical lines.

The magnetization  $|\langle \sigma_x \rangle|$  can be regarded as the order parameter in the ASBM. Color plots for the magnetization  $|\langle \sigma_x \rangle|$  are displayed in the middle panel and the entanglement entropy  $S_E$  between the two-level system and the environment bath are exhibited in the lower panel. It is remarkable to see that the skeleton of the phase diagram can be directly obtained from the color plot of the

entropy. The order parameter share the common shape with the phase boundary marked by the red dashed line. We will describe these results in detail below.

In its prototype spin boson model, the 2nd-order QPT from the delocalized to localized phases has been well known for a long time. This conventional picture also applies to the ASBM at small power of the spectral function, e. g.  $s = 0.3$ , where the phase diagram only consists of two phases (I and III), as shown in the upper right panel of Fig. 1. This phase diagram can be replot in the similar way as that in the anisotropic Dicke model [11], c.f. their Fig. 2.

Surprisingly, for  $s > 1/2$ , e.g.  $s = 0.7$ , a new delocalized phase with odd parity (phase II) can grow at the phase III region and having a common border with phase I, as exhibited in the upper left panel of Fig. 1. It intervenes between phases I and III in an unusually way. The QPT from the two delocalized phase is of 1st-order due to the level crossing caused by the different wavefunctions with opposite parities, whereas the QPTs from any delocalized phase to localized phase are definitely of the 2nd-order due to the symmetry breaking.

For the highly anisotropic case, both the 1st- and 2nd-order QPTs take place successively from phases I to II, then to phase III, similar to the SBM in the RWA. Note however that the total excitation in the ASBM is not conserved, unlike the SBM in the RWA. Especially in the moderate anisotropic model, with increasing coupling strength, the system would undergo the 2nd-order QPTs for three times:  $I \rightarrow III$ ,  $III \rightarrow II$ , and  $II \rightarrow III$ . This unusual reentrance to the same localized phase has never been reported before in the light-matter interaction systems.

To study the QPTs deeply, we will discuss the order parameter and the entanglement entropy in detail in the next subsections. For more clear, we extract the data of the parity, magnetization, and the entropy as a function of coupling strength  $\alpha$  at  $\lambda = 0.3$  and  $0.9$  in Fig. 1, and re-plot them in Fig. 2 for  $s = 0.7$  and Fig. 3 for  $s = 0.3$ , respectively.

## B. Order parameter

Generally, in the delocalized phase, spin has the equal probability in the two states, spin-up and spin-down (both in  $x$ -axis here), while in localized phase, spin prefers to stay in one of the two states. Because phases I and II are delocalized ones with opposite parities ( $\pm 1$ ), the order parameter must be zero due to symmetry. So we cannot distinguish phase II from phase I by the order parameter, which is shown in the blue regime of the middle left panel of Fig. 1. Non-zero order parameter is only found in the localized phase due to symmetry breaking. The parity always jumps to different plateaus when crossing any phase boundaries. These characteristics are clearly shown in upper panels in Figs. 2 and 3, which can be used to compose the phase diagram precisely.

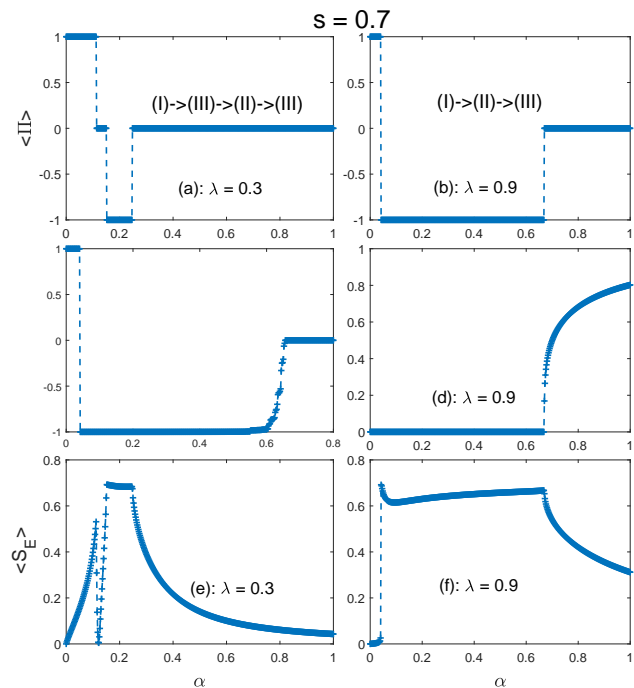


FIG. 2: (Color online) Parity  $\langle \Pi \rangle$  (upper panels), magnetization  $|\langle \sigma_x \rangle|$  (middle panels), and entanglement entropy  $\langle S_E \rangle$  (lower panels) as a function of  $\alpha$  in the ground state for  $\lambda = 0.3$  (left) and  $\lambda = 0.9$  (right) by VMPS approach.  $\Delta = 0.1$ ,  $\omega_c = 1$ ,  $\epsilon = 0$ ,  $\Lambda = 2$ ,  $L = 50$ ,  $d_{opt} = 12$ , and  $D = 40$  for  $s = 0.7$ .

One can indeed see that the order parameter remains zero in the phase I and II and only become nonzero in the phase III in the middle panels of Figs. 2 and 3. The remarkable peak of order parameter in the middle left of Fig. 2 for  $s = 0.7$ ,  $\lambda = 0.3$  is originated from the narrow localized phase III.

For small power of the spectral function, say  $s = 0.3$ , there only exists two phases: delocalized phase with even parity I and localized phase III. Although the phase II does not show up in the phase diagram for small  $s$ , it still plays some role. The magnetization for different anisotropy shows different behaviors after the critical point in the middle panel of Fig. 3 for  $\lambda = 0.3$  and  $0.9$ . For  $\lambda = 0.3$ , the order parameter increases monotonously to the global maximum, while for  $\lambda = 0.9$ , it displays a nonmountainous behavior with  $\alpha$ . One can find in the phase diagram that the high anisotropy  $\lambda$  and large  $s$  favor the emergence of phase II. Even for small  $s$ , phase II finally disappears due to the lost in the competition with phase III, but its effect would not disappear completely without a trace. According to the different symmetry, it is to note that phase III enhances but phase II suppresses the magnetization, which cooperate to result in the local minimum of the magnetization in this region. Of courses, if phase II somehow truly appears in this region, the magnetization must be zero, no any the local minimum can be seen.

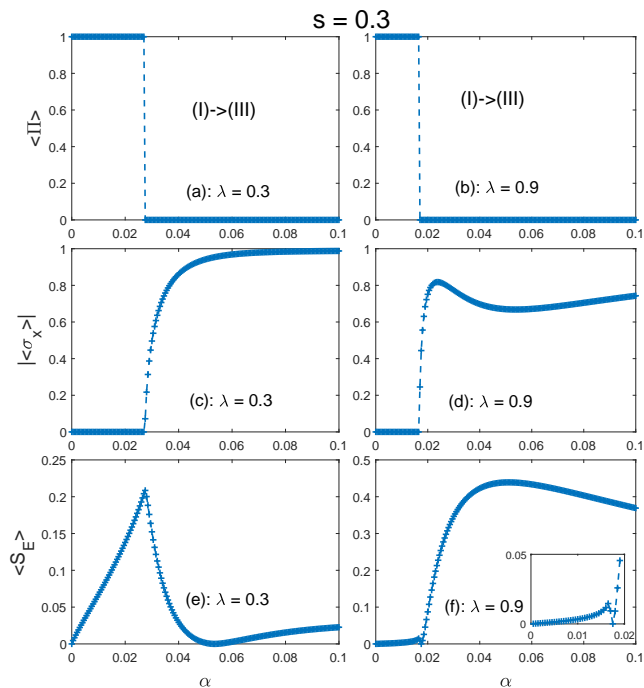


FIG. 3: (Color online) Parity  $\langle \Pi \rangle$  (upper panels), magnetization  $|\langle \sigma_x \rangle|$  (middle panels), and entanglement entropy  $\langle S_E \rangle$  (lower panels) as a function of  $\alpha$  in the ground state for  $\lambda = 0.3$  (left) and  $\lambda = 0.9$  (right) by VMPS approach.  $\Delta = 0.1$ ,  $\omega_c = 1$ ,  $\epsilon = 0$ ,  $\Lambda = 2$ ,  $L = 50$ ,  $d_{opt} = 12$ , and  $D = 20$  for  $s = 0.3$ .

### C. Entanglement Entropy

The entanglement entropy  $S_E$  is presented in the low panel of Fig. 1 for  $s = 0.7$  and  $0.3$ . From the low panels of Figs. 2 and 3, we can observe that the entropy changes drastically when crossing all 1st- and 2nd-order critical lines. As shown in Ref. [43] in the fermionic systems, the entanglement can be used to identify quantum phase transitions. So, the implications between the entanglement and the quantum phase in the present ASBM should be also nontrivial.

To shed some insights, we first consider the 1st-order QPT in the SBM in the RWA ( $\lambda = 1$ ) [35]. In this case, the total excitation  $\hat{N} = \sum_k a_k^\dagger a_k + \sigma_+ \sigma_-$  is the conserved number. At the weak coupling,  $\langle N \rangle = 0$ , corresponding to even parity  $\langle \Pi \rangle = 1$ , the ground state wave-function is  $|\psi_0\rangle = |0\rangle |\downarrow\rangle$  with energy  $E_0 = -\frac{\Delta}{2}$ , then we can obtain the reduced density matrix for spin

$$\rho_{spin} = |\downarrow\rangle \langle \downarrow|,$$

one can easily obtain entropy  $S_E = 0$  from Eq. (8).

When exceeding the 1st QPT point,  $\langle N \rangle$  jumps to 1 corresponding to odd parity  $\langle \Pi \rangle = -1$ , the ground state wave-function for the single excitation is

$$|\psi_1\rangle = c |0\rangle |\uparrow\rangle + \sum_k d_k a_k^\dagger |0\rangle |\downarrow\rangle, \quad (9)$$

where  $c$  and  $d_k$  are the coefficients for the bosonic vacuum and single boson number states. One can easily obtain  $c^2 = (1 + \langle \sigma_z \rangle) / 2$ . The reduced density matrix for the spin is

$$\rho_{spin} = c^2 |\uparrow\rangle \langle \uparrow| + (1 - c^2) |\downarrow\rangle \langle \downarrow|. \quad (10)$$

If  $\langle \sigma_z \rangle = 0$ , we obtain the maximum entropy  $S_E^{\max} = \log 2 = 0.693$  from Eq. (8). In this case, the probabilities of spin-up and spin-down are equal, corresponding to the largest entanglement between spin and bath. In the single excitation state  $\langle \sigma_z \rangle$  is usually small. e.g. it is found in Fig. 2(b) of our previous work [35] that  $\langle \sigma_z \rangle$  suddenly switches to a small value around  $0.3 \pm 0.1$  when crossing the 1st-order QPT point. The entropy in the single excitation state can be larger than 0.6.

In the presence of the counter rotating wave terms in the ASBM, the total excitation  $\hat{N}$  is no longer conserved. The state with the even parity at the weak coupling is not  $|\psi_0\rangle = |0\rangle |\downarrow\rangle$  any more, the even  $\hat{N}$  components in the states would be involved gradually with the coupling strength, so the entropy increases within phase I, consistent with the numerical calculations shown in the low panels of Figs. 2 and 3.

The parity would be possibly the odd one with the increase of the coupling strength, such as phase II. As long as  $\lambda \neq 1$ , the state is different from but close to the state (9) with a single excitation. So the entropy is also high in phase II. We indeed find that the entropy in all phase II regime is high, indicating it is a highly entangled phase. As shown in the low left panel of the Fig. 1, a highly entanglement regime appears in the phase II area. In the 1st-order QPT boundary from phase I and II, the entropy jumps suddenly to a value close to  $S_E^{\max}$  in phase II, as is just shown in the lower right of Fig. 2 at  $s = 0.7$ ,  $\lambda = 0.9$ .

In the localized phase III of the isotropic SBM, Chin *et al.* find a monotonic decrease of entanglement above the transition by means of the nonadiabatic modes [30] analytically, consistent with the numerical calculations [44]. In the present ASBM, this behavior may be modified due to the competition with "invisible" phase II, which is lacking in the isotropic SBM but still possible in the present ASBM. In the phase III region of the lower panel of Fig. 3 for  $s = 0.3$ , at  $\lambda = 0.3$  and  $0.9$ , we note that the entropy decreases first, reaches a local minimum, and surprisingly rises again when the coupling strength increases further, in contrast to the isotropic SBM. As discussed in the last subsection, the phase III competes with phase II in this area and wins finally. Although phase II finally cannot come out, it could still enhance the entanglement. The observed local minimum is just caused by the cooperated effect of the competition of phase II and III beyond of the weak coupling. We have confirmed that, in the strong coupling limit, the entropy in all cases must vanish (not shown here).

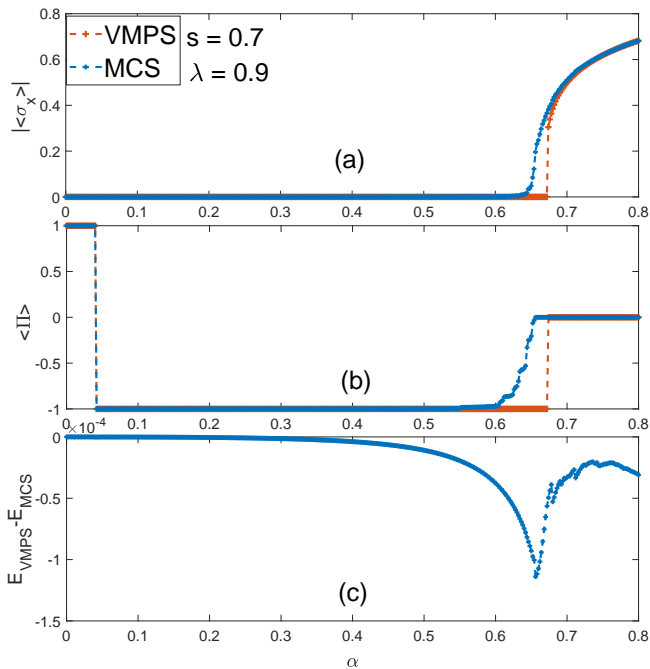


FIG. 4: (Color online) (a) The order parameter  $|\langle\sigma_x\rangle|$ , (b) the parity  $\langle\Pi\rangle$  as a function of the coupling strength within VMPS and MCS variational approaches. (c) The difference between the VMPS ground-state energy and that by MCS.  $s = 0.7$ ,  $\lambda = 0.9$ ,  $\Delta = 0.1$ ,  $\omega_c = 1$ ,  $\epsilon = 0$ ,  $\Lambda = 2$ ,  $L = 20$ ,  $d_{opt} = 12$ ,  $D = 20$ ,  $N_c = 9$ .

#### D. Evidence for 1st-order QPT between the phases with opposite parities by MCS variational studies

The most interesting observation in the ASBM is that a new phase II with odd parity intervenes between the usual phase I and III, which is absent in the isotropic SBM. To provide another evidence of this new quantum phase, we also employ the MCS approach here. By VMPS, for  $s = 0.7$  and  $\lambda = 0.9$ , we have observed that a large region of phase II appears between the phase I and III. Since all the three phases can be described well in the trial wave function (6), we in principle can detect these phases in the MCS framework. In Fig. 4, we list results for parity magnetization ground-state energy by both MCS and VMPS approaches for  $s = 0.7$  and  $\lambda = 0.9$ . Notice that only  $L = 20$  bosonic modes are taken for both approaches here due to the computational difficulties in the MCS approach. However, it does not influence the essential results at all. All the results in the large phase II regime by both approaches are almost consistent, convincingly demonstrating the existence of the phase II regime according to its characteristics. The wavefunction in the MCS reproduce the phase II with the odd parity explicitly by noting  $A_n = -B_n$ . The deviation of the results in the transition regime from Phase II and III is indeed visible, but it does not influence the

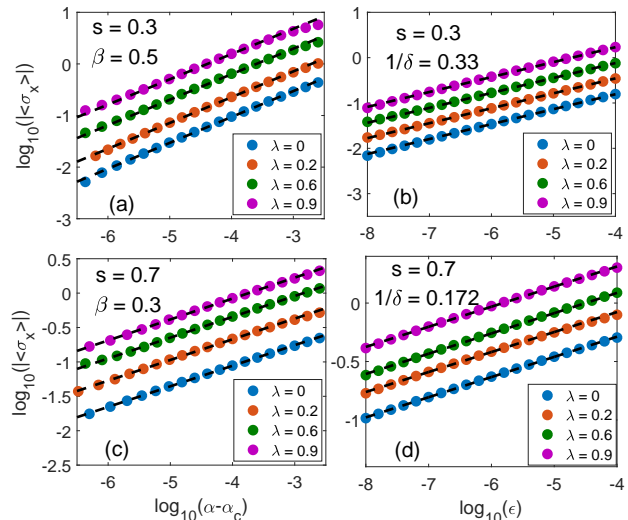


FIG. 5: (Color online) The log-log plot of the magnetization  $|\langle\sigma_x\rangle|$  as a function of  $\alpha - \alpha_c$  (left) at  $\epsilon = 0$  and bias  $\epsilon$  (right) at  $\alpha = \alpha_c$  of the ASBM for  $s = 0.3$  (upper panel) and  $s = 0.7$  (lower panel). The numerical results by VMPS are denoted by blue, orange, green, purple circles for  $\lambda = 0, 0.2, 0.6, 0.9$  respectively, and the power-law fitting curves are denoted by the black dashed lines, which shows  $\beta = 0.5, 0.3$  and  $1/\delta = 0.33, 0.172$  for  $s = 0.3, 0.7$  respectively. For visibility, the curves for different  $\lambda$  have been shifted to distinguish them.  $\Delta = 0.1, \omega_c = 1$ ,  $\Lambda = 2$ ,  $L = 50$ ,  $d_{opt} = 12$ , and  $D = 20, 40$  for  $s = 0.3, 0.7$  respectively.

existence of phase II. We should point out that the MCS approach is used here to provide another piece of evidence for the existence of phase II qualitatively, not for the precise location of the critical points.

#### E. The critical exponent for the order parameters

The critical behavior of the 2nd-order QPT from phase I to III and from phases II to III, such as the critical exponents  $\beta$  and  $\delta$  will be also discussed in this subsection. We present the log-log plot of the magnetization  $|\langle\sigma_x\rangle|$  as a function of  $\alpha - \alpha_c$  at  $\epsilon = 0$  and bias  $\epsilon$  at  $\alpha = \alpha_c$  for  $s = 0.3$  and  $s = 0.7$  with different anisotropic parameter  $\lambda = 0, 0.2, 0.6, 0.9$  in the critical regime in Fig. 5. The critical exponents  $\beta$  and  $\delta$  can be determined by fitting power-law behavior,  $|\langle\sigma_x\rangle| \propto (\alpha - \alpha_c)^\beta$  with the bias  $\epsilon = 0$  and  $\langle\sigma_x\rangle \propto \epsilon^{1/\delta}$  at the critical coupling strength  $\alpha = \alpha_c$ . Surprisingly, all the critical exponents of the anisotropic model show the same rules compared to the isotropic SBM, where it takes the mean-field value  $\beta = 1/2, 1/\delta = 1/3$  for  $s < 1/2$  and the hyperscaling  $\beta < 1/2, 1/\delta = (1 - s)/(1 + s)$  for  $s > 1/2$ .

Apart from the last 2nd-order QPTs from the conserved parity phase to the phase III, for large  $s$  at the moderate anisotropy, several 2nd-order QPTs may happen with the increase of the coupling strength. We also

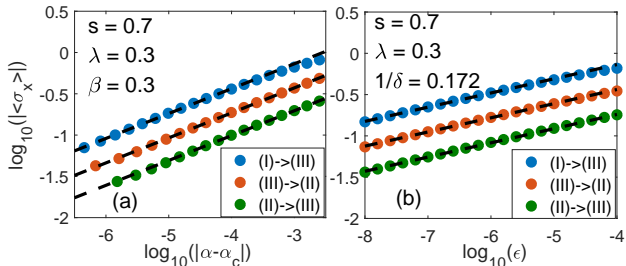


FIG. 6: (Color online) The log-log plot of the magnetization  $|\langle \sigma_x \rangle|$  as a function of  $|\alpha - \alpha_c|$  (left) at  $\epsilon = 0$  and bias  $\epsilon$  (right) at  $\alpha = \alpha_c$  of the ASBM for  $s = 0.7, \lambda = 0.3$ . The numerical results by VMPS are denoted by blue, orange, green, circles for the critical processes (I) to (III), (III) to (II) and (II) to (III) respectively, and the power-law fitting curves are denoted by the black dashed lines, which shows  $\beta = 0.3$  (left) and  $1/\delta = 0.172$  (right) for 0.7 respectively. For visibility, the curves for different  $\lambda$  have been shifted to distinguish them.  $\Delta = 0.1, \omega_c = 1, \Lambda = 2, L = 50, d_{opt} = 12$ , and  $D = 40$  for  $s = 0.7$  respectively.

evaluate the critical exponents for these multiple 2nd-order QPTs for  $s = 0.7, \lambda = 0.3$  in Fig. 6. Very surprisingly, the same critical exponents  $\beta$  and  $\delta$  are obtained, indicating that they belong to the same universality class. Based on these observations, we can say that, counter-rotating terms would almost have no effect on critical exponents even when several 2nd QPTs are present successively at a few critical points for fixed anisotropy in the ASBM.

The universality in the quantum tricritical point in the ASBM is a very challenging issue. According to the Landau theory, it should be different from those in other critical points. The numerical calculations cannot be used to distinguish this isolated point from others, and much less the universality. The analytical treatment is, however, lacking in any SBMs except in the Ohmic bath, unlike the Dicke models [7, 11, 13]. A field theory formulated from the Feynman path-integral representation of the partition function for the SBM [5, 45–47] might be extended to the ASBM. Then analytical arguments based on the quantum-to-classical mapping would be helpful to clarify this issue.

## IV. CONCLUSION

We have found rich quantum phases in the ASBM with the sub-Ohmic bath by the VMPS approach. The phase diagram has been composed in the coupling strength and anisotropy space. For large power of the spectral function, two 2nd-order QPT critical lines meet the 1st-order QPT line at the same point, a quantum tricritical point. At any 2nd-order QPT lines, the critical exponent of the order parameter and its the field related critical exponents are the same, which only depend on the power of the spectral function. All phase boundaries can be precisely determined by the parity and the entanglement entropy, besides, the 2nd-order QPTs can be also detected by the magnetization. The 1st-order QPTs between opposite parity symmetry have been corroborated by the MCS approach where we can directly observe the opposite parity in the ground-state wavefunction. For low power of the spectral function, the system only experiences the 2nd-order QPT from the delocalized to localized phases, similar to that in the isotropic SBM.

The newly found symmetric quantum phase with the odd parity emerges in the localized phase region and is border to the phase with even parity, which enriches the critical phenomena in the spin and boson coupling systems. Although this phase share the same odd parity with the phase in the single excitation in the SBM under the RWA, the total excitation number is not conserved. The QPT to the localized phase from a delocalized phase with odd parity has never been found before in the SBM. The ASBM might be realized in the superconducting circuit QED system where the anisotropic parameters can be manipulated artificially, We believe that the ASBM would serve as a new important lab to study the rich quantum criticality.

**ACKNOWLEDGEMENTS** This work is supported by the National Science Foundation of China (Nos. 11834005, 11674285), the National Key Research and Development Program of China (No. 2017YFA0303002),

\* Email:qhchen@zju.edu.cn

---

[1] S. Sachdev, *Quantum Phase Transitions*, 2nd ed. (Cambridge University Press, Cambridge, England, 2011).  
 [2] V. J. Emery in *Highly Conducting One-Dimensional Solids*, edited by J.T. Devreese et al. (Plenum, New York, 1979), pp. 247–303; J. Solyom, *Adv. Phys.* **28**, 201 (1979); H.-Q. Lin et al., in *The Hubbard Model: Its Physics and Mathematical Physics*, edited by D. Baeriswyl, pp. 315–327.  
 [3] M. Greiner, O. Mandel, T. Esslinger, T. W. Haensch, and I. Bloch, *Nature(London)* **415**, 39 (2002).  
 [4] E. Fradkin and J. E. Hirsch, *Phys. Rev. B* **27**, 1680

(1983); W.-Q. Ning, H. Zhao, C.-Q. Wu, and H.-Q. Lin, *Phys. Rev. Lett.* **96**, 156402 (2006); E. A. Nowadnick, S. Johnston, B. Moritz, R. T. Scalettar, and T. P. Devreese, *Phys. Rev. Lett.* **109**, 246404 (2012).  
 [5] A. J. Leggett, S. Chakravarty, A. T. Dorsey, M. P. A. Fisher, A. Garg, and W. Zwerger, *Rev. Mod. Phys.* **59**, 1(1987).  
 [6] M.-J. Hwang, R. Puebla, and M. B. Plenio, *Phys. Rev. Lett.* **115**, 180404 (2015); M. X. Liu, S. Chesi, Z.-J. Ying, X. S. Chen, H.-G. Luo, H.-Q. Lin, *Phys. Rev. Lett.* **119**, 220601 (2017).

- [7] R. H. Dicke, Phys. Rev. **93**, 99 (1954); C. Emary and T. Brandes, Phys. Rev. E **67**, 066203 (2003) ; Phys. Rev. Lett. **90**, 044101 (2003); Q.-H. Chen, Y.-Y. Zhang, T. Liu, and K.-L. Wang, Phys. Rev. A **78**, 051801 R (2008); T. Liu, Y.-Y. Zhang, Q.-H. Chen, and K.-L. Wang, Phys. Rev. A **80**, 023810(2009).
- [8] R. Bulla, N. Tong, and M. Vojta, Phys. Rev. Lett. **91**, 170601 (2003); M. Vojta, N. Tong, and R. Bulla, Phys. Rev. Lett. **94**, 070604 (2005); R. Bulla, Phys. Rev. Lett. **102**, 249904(E) (2009).
- [9] Q. Si et al., Nature (London) **413**, 804 (2001); Phys. Rev. B **68**, 115103 (2003).
- [10] J. Ye and C. L. Zhang, Phys. Rev. A **84**, 023840 (2011).
- [11] A. Baksic and C. Ciuti, Phys. Rev. Lett. **112**, 173601 (2014).
- [12] Z. Q. Zhang, C. H. Lee, R. Kumar, K. J. Arnold, S. J. Masson, A. L. Grimsmo, A. S. Parkins, and M. D. Barrett, Phys. Rev. A **97** 043858 (2018).
- [13] Y. Xu and H. Pu, Phys. Rev. Lett. **122**, 193201 (2019).
- [14] R. B. Griffiths, Phys. Rev. Lett. **24**, 715 (1970).
- [15] M. O. Scully and M. S. Zubairy, *Quantum Optics* (Cambridge University Press, Cambridge, 1997).
- [16] H. P. Breuer and F. Petruccione, *The Theory of Open Quantum Systems* (Oxford University Press, New York, 2002).
- [17] U. Weiss, *Quantum Dissipative Systems* (World Scientific Publishing Company, 2008).
- [18] T. Niemczyk et al., Nature Physics **6**, 772 (2010).
- [19] F. Yoshihara, T. Fuse, S. Ashhab, K. Kakuyanagi, S. Saito, and K. Semba, Nat. Phys. **13**, 44 (2017).
- [20] F. Dimer, B. Estienne, A. S. Parkins, and H. J. Carmichael, Phys. Rev. A **75**, 013804 (2007); K. Baumann, C. Guerlin, F. Brennecke, and T. Esslinger, Nature (London) **464**, 1301 (2010).
- [21] J. I. Cirac, A. S. Parkins, R. Blatt, and P. Zoller, Phys. Rev. Lett. **70**, 556 (1993).
- [22] P. Forn-Díaz, J. J. García-Ripoll, B. Peropadre, J.-L. Orgiazzi, M. A. Yurtalan, R. Belyansky, C. M. Wilson, and A. Lupascu, Nat. Phys. **13**, 39 (2017).
- [23] J. Keeling, M. J. Bhaseen, and B. D. Simons, Phys. Rev. Lett. **105**, 043001 (2010).
- [24] Q. T. Xie, S. Cui, J. P. Cao, L. Amico, and H. Fan, Phys. Rev. X **4**, 021046 (2014).
- [25] A. L. Grimsmo and S. Parkins, Phys. Rev. A **87** 033814 (2013).
- [26] A. Winter, H. Rieger, M. Vojta, and R. Bulla, Phys. Rev. Lett. **102**, 030601 (2009).
- [27] A. Alvermann and H. Fehske, Phys. Rev. Lett. **102**, 150601 (2009).
- [28] M. Vojta, R. Bulla, F. Güttge, and F. Anders, Phys. Rev. B **81**, 075122 (2010).
- [29] Y.-Y. Zhang, Q.-H. Chen, and K.-L. Wang, Phys. Rev. B **81**, 121105(R)(2010).
- [30] A. W. Chin, J. Prior, S. F. Huelga and M. B. Plenio, Phys. Rev. Lett. **107**, 160601 (2011).
- [31] C. Guo, A. Weichselbaum, J. von Delft, and M. Vojta, Phys. Rev. Lett. **108**, 160401 (2012).
- [32] M. F. Frenzel and M. B. Plenio, New Journal of Physics **15**, 073046(2013).
- [33] C. R. Duan, Z. F. Tang, J. S. Cao, and J. L. Wu, Phys. Rev. B **95**, 214308 (2017).
- [34] S. He, Li. W. Duan, and Q. -H. Chen, Phys. Rev. B **97**, 115157 (2018).
- [35] Y.-Z. Wang, S He, L.-W. Duan, Q.-H. Chen. Phys. Rev. B **100**, 115106 (2019).
- [36] A. W. Chin, A. Rivas, S. F. Huelga, and M. B. Plenio, Journal of Mathematical Physics **51**, 092109 (2010).
- [37] F. A. Y. N. Schröder, A. W. Chin, Phys. Rev. B **93**, 075105 (2016).
- [38] A. Weichselbaum, F. Verstraete, U. Schollwöck, J. I. Cirac, and J. von Delft, Phys. Rev. B **80**, 165117 (2009).
- [39] H. Saberi, A. Weichselbaum, and J. von Delft, Phys. Rev. B **78**, 035124 (2008).
- [40] S. Bera, S. Florens, H. U. Baranger, N. Roch, A. Nazir, A. W. Chin, Phys. Rev. B **89**, 121108(R) (2014); S. Bera, A. Nazir, A. W. Chin, H. U. Baranger, S. Florens, Phys. Rev. B **90**, 075110 (2014).
- [41] L. Duan, S. He, Q.-H. Chen, arXiv:1412.6343.
- [42] Z. Blunden-Codd, S. Bera, B. Bruognolo, N.-O. Linden, A. W. Chin, J. von Delft, A. Nazir, and S. Florens, Phys. Rev. B **95**, 085104 (2017).
- [43] S. -J. Gu, S. -S. Deng, Y. -Q. Li, and H. -Q. Lin, Phys. Rev. Lett. **93**, 086402 (2004).
- [44] K. Le Hur, P. Doucet-Beaupre and W. Hofstetter, Phys. Rev. Lett. **99**, 126801 (2007).
- [45] M. Vojta, Phys. Rev. B **85**, 115113 (2012)
- [46] S. Kirchner, J. Low Temp. Phys. **161**, 282 (2010).
- [47] S. Kirchner, Q. Si, and K. Ingersent, Phys. Rev. Lett. **102**, 166405 (2009); S. Kirchner, K. Ingersent, and Q. Si, Phys. Rev. B. **85**, 075113(2012).